Journal of Environmental Management 341 (2023) 118057

Contents lists available at ScienceDirect

Journal of Environmental Management

journal homepage: www.elsevier.com/locate/jenvman

Research article

Evaluation of compressive strength and phosphate fixation characteristics of wastewater filter media using coal bottom ash and oyster shells

Ilwon Jeong [a], Kyunghoi Kim [b,c,*]

[a] Research Center for Ocean Industrial Development, Department of Ocean Engineering, Pukyong National University, Busan, 48513, South Korea
[b] Department of Ocean Engineering, Pukyong National University, Busan, 48513, South Korea
[c] Department of Biology, Faculty of Science and Technology, Universitas Airlangga, Surabaya, 60115, Indonesia

ARTICLE INFO

Keywords:
Coal bottom ash
Oyster shells
Filter media
Compressive strength
Phosphate fixation

ABSTRACT

The excessive concentration of phosphate in coastal areas results in environmental problems such as red tide and eutrophication. Filter media (FM) is used in wastewater treatment facilities to decrease phosphate concentration. This study aims to investigate the optimal mixing ratio for high compressive strength and phosphate fixation ability using coal bottom ash (CBA) and oyster shells (OS) -derived FM. Compressive strength experiments were conducted using mixed CBA and OS with different mixing ratios, 1:3 (GBO13), 1:1 (GBO11), and 3:1 (GBO31). The highest compressive strength of 0.93 MPa was observed in GBO11. GBO11 had similar elemental proportions with Portland cement, promoting a pozzolanic reaction and forming calcium-silicate-hydrate. The phosphate fixation capability of GBO11 was evaluated through an up-flow column filtration experiment. GBO11 fixed phosphate through precipitation and adsorption, and the maximum amount of phosphate fixation was estimated to be 1.403 mg-P/g. This study demonstrates that the combination of CBA and OS can be promising FM with high compressive strength and phosphate fixation properties.

1. Introduction

Phosphate is discharged from the agriculture and livestock industries' wastewaters into rivers and coastal areas. Increased phosphate concentration in water bodies can cause eutrophication, harmful algal blooms, decreased oxygen levels, and eventually aquatic ecosystem devastation. Therefore, managing the introduction of phosphate is critical for maintaining a healthy aquatic environment.

Fixation using a porous filtration medium (FM) is a well-known method with high efficiency and low cost for phosphate fixation in water (Ruby et al., 2015; Wu et al., 2021). However, while several researchers have developed new FMs, several problems have consistently been encountered. For example, there is a relatively low phosphate fixation efficiency from natural FM such as sand (Vidal et al., 2018), high production costs from synthetic FMs such as zeolite-sand (Bruch et al., 2011), microplastic generation from plastic FM (Luis et al., 2021), low fluid flow, and difficulty in sludge separation from powdery FM (Li et al., 2022).

Backwashing of FM due to biofilm formation on the outer FM surface (Jeong et al., 2022; Mauclaire et al., 2004; Roychand et al., 2020), and the periodic replacement of FM add to the maintenance costs. In addition, the Government has tried to find affordable local sources of FM because of their high import costs (Mustapha et al., 2021). Hence, a novel porous FM is needed to satisfy key requirements such as high phosphate fixation efficiency, environmentally friendly materials, low production cost, easy shaping, and lightweight materials for transportation.

This study selected coal bottom ash (CBA) and oyster shells (OS) as the raw materials for a novel porous FM. CBA and OS are environment-friendly materials that are potential wastewater absorbents due to their relatively high phosphate fixation efficiencies (Jeong et al., 2019; Rashidi and Yusup, 2016; Shih and Chang, 2015; Yan et al., 2007). In addition, porosity structures in both CBA and OS are expected to show higher phosphorus fixation efficiency (Abdulmatin et al., 2018; Hellen et al., 2019).

Approximately 730 million tons of CBA and 3 million tons of OS have been generated annually as by-products of coal power plants and the fishing industry, respectively (Abbas et al., 2020; Hellen et al., 2019; Maeng et al., 2015). Both materials can be used as concrete admixtures and aggregates (Hellen et al., 2019; Maeng et al., 2015). Furthermore, considering the need for recycling waste materials, CBA and OS can be utilized as low-cost FM (Rashidi and Yusup, 2016; Shih and Chang,

* Corresponding author. Department of Ocean Engineering, Pukyong National University, Busan, 48513, South Korea.
E-mail addresses: jeongiw@pknu.ac.kr (I. Jeong), hoikim@pknu.ac.kr (K. Kim).

https://doi.org/10.1016/j.jenvman.2023.118057
Received 22 March 2023; Received in revised form 20 April 2023; Accepted 27 April 2023
Available online 5 May 2023

2015), with easy molding potential.

A combination of CBA and OS may overcome the FM limitations mentioned above. Recently, it has been reported that a mixture of CBA and OS, called granulated coal bottom ash and oyster shells (GBO), can act as an *in-situ* capping material in contaminated coastal sediments and effectively decrease the phosphate concentration (Jeong and Kim, 2022). However, the compressive strength and the phosphate fixation efficiency of these CBA and OS mixtures have yet to be quantitatively evaluated.

Therefore, this study aims to determine the best mixing ratio for high compressive strength and phosphate fixation efficiency from a CBA and an OS-derived FM.

2. Materials and methods

2.1. Pretreatment of materials

CBA was collected from a bottom ash landfill at the Samcheonpo thermal power plant. The collected CBA was pyrolyzed at 600 °C for 6 h to remove residue and organic matter. To improve the pozzolanic reactivity of the CBA, it was initially pulverized to increase its specific surface area and silica content. (Al Biajawi et al., 2022). OS was collected from landfills of oyster industries in Tongyeong-si, and washed with tap water. The cleaned OS was dried at 100 °C for 6 h and pulverized. Calcium carbonate ($CaCO_3$) is the main chemical component in OS. To convert $CaCO_3$ to calcium oxide (CaO), the OS was pyrolyzed at 800 °C for 6 h (Jeong et al., 2020). X-ray fluorescence (XRF) analysis (Shimadzu XRF-1800) was conducted to confirm the changes in the chemical composition of the CBA and OS before and after pyrolysis (Table 1). These results indicated that the main chemical elements of CBA and OS are silicon dioxide (SiO_2) and CaO, respectively, which increased after pyrolysis.

The loss on ignition (LOI) of CBA and OS was measured through weight differences between the samples after pyrolyzing at 600 °C for 4 h. The weight difference was 6.8% for CBA and 3.5% for OS. Although no LOI criteria exist for OS, the LOI of CBA exceeded 6%, a criterion for Class F materials (Hasim et al., 2022). Pulverized CBA and OS were sieved (NO. 18 sieve, ATSM) to obtain a fine residue powder under 1 mm in size. The particle size distribution and specific surface area of CBA and OS were determined using a particle size analyzer (Mastersizer 3000, Malvern Panalytical) and a surface area analyzer (Quantachrome, Autosorb-iQ), respectively.

To produce granulated CBA and OS (GBO), CBA and OS were mixed at three different weight ratios: 1:3 (GBO13), 1:1 (GBO11), and 3:1 (GBO31). A particle size distribution of the GBOs shows that the D_V (50) of the GBOs ranges from approximately 0.28–0.30 mm, corresponding to medium sand (0.25–0.5 mm) (Blair and McPherson, 1999). In addition, X-ray diffraction (XRD) analysis (PANalytical, X'Pert-powder) and XRF analysis were conducted to determine the chemical crystallographic structures and compositions of the GBOs.

2.2. Unconfined uniaxial compressive experiment

The GBOs and tap water were mixed in a 1 : 0.6 by weight ratio. The workable mixtures of each GBO were filled into 15 cylindrical molds (D: 5 cm, H: 10 cm). All cylinders (n = 45) were intermittently sprayed with tap water for 48 h to prevent the surface from drying. Subsequently, each cylindrical mold was unveiled one week after casting and cured for 2–6 weeks. Unconfined uniaxial compressive strength tests were performed every week for the three cylinders with dry surface conditions on GBO13, GBO11, and GBO31.

Changes in the compressive strength were measured using a digital compression testing machine (DA-505, Digicom Unconfined Compression Tester, Dong Ah Testing machine). Displacement-controlled loading was applied at a uniform rate of 1 mm/min to a GBO cylinder. The maximum load was measured when the brittle fracture occurred. The average value from compressive expreiments was used as a representative value.

Table 1
Chemical composition changes in CBA and OS.

Content	CaO	SiO_2	Al_2O_3	Fe_2O_3	MgO	TiO_2	SO_3	K_2O
Raw CBA (%)	4.9	62.9	19.2	3.9	2.6	1.2	0.6	1.5
Pyrolyzed CBA (%)	4.4	65.8	17.6	3.6	2.7	–	2.2	1.7
Dried OS (%)	95.2	0.6	0.2	0.1	0.8	–	0.9	–
Pyrolyzed OS (%)	99.3	–	–	–	–	–	0.6	–

2.3. Up-flow column filtration experiment

GBO11 was selected to evaluate its phosphate fixation ability because it has already shown high compressive strength and phosphate fixation potential (Jeong and Kim, 2022). GBO11 was ball-shaped and cured for a month. The diameter of GBO11 ranged from 1 cm to 2.5 cm, and its density was 1140 kg/m^3, which is lighter than P. II 42.5 R ordinary Portland cement (density of 3150 kg/m^3).

The up-flow column filtration method was used to evaluate the GBO11 phosphate fixation ability (Fig. 1). A 25 mg/L phosphate solution was prepared using KH_2PO_4 (Sigma-Aldrich, Japan) and ultra-pure water (Ultima Duo 200, Balmann Tech). The phosphate solution was stored in a 25 L polyethylene influent tank that was continuously refilled. A column (D: 113 mm, H: 150 mm, thickness: 3 mm, polyvinyl chloride pipe) was prepared and filled with 890 g of GBO11. During the experimental period, the influent (phosphate solution) was pumped through the column at a flow rate of 300 mL/min for 3 min every 6 h, using a timer-controlled peristaltic pump (BT600-2 J, Longer Pump) with a hydraulic retention time of 6 h. The effluent was collected immediately for analysis. The pH, oxidation-reduction potential (ORP), and PO_4–P concentrations in the influent and GBO11 effluent were measured in triplicate. The pH and ORP were measured using a pH/ORP/Ion meter (LAQUA F-73, Horiba). The PO_4–P concentration was measured using a spectrophotometer (DR 3900, Hach). The filtration experiment was conducted continuously for two weeks until 50 effluent solutions were collected (approximately 315 h).

The cumulative amount of P fixation was calculated based on changes in the PO_4–P concentration. The amount of fixed P (mg of P per gram of GBO11) was calculated using the mass of adsorbed P (mg) and the weight of GBO11 (g). In addition, a second-order polynomial regression equation of the P fixation amount was used to determine the maximum P fixation amount and replacement cycle of GBO11.

2.4. Statistical analysis

The obtained data were analyzed and treated using Excel and Origin 2021b. Data organization, and calculation of mean and standard deviation values were performed using Excel. After then, the data variation

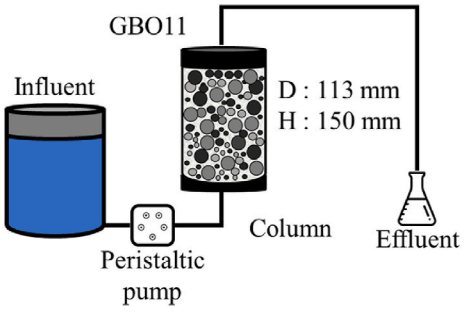

Fig. 1. Schematic diagram of the up-flow filtration test.

was plotted as the bar chart and scatter chart by Origin 2021b. One-way analysis of variance (ANOVA) in Origin 2021b was applied among GBO13, GBO11, and GBO31, and significance levels were set as p-value <0.05. In addition, the features of the scatter plot in Origin 2021b were used to visualize the second polynomial regression equation.

3. Results and discussion

3.1. Physiochemical properties of CBA and OS

The particle size distribution of the CBA was finer than that of the OS (Fig. 2). CBA is brittle because of its porous structure, which results in finer particles during pulverization. In contrast, OS is a porous material, it consists of thin layer sheets, called "Folia" (Lee et al., 2008). This specific structure of OS minimized the external structural force and resulted in larger particle sizes than pulverized CBA.

XRD in the GBOs shows that quartz (ICSD #156198; SiO_2), calcite (ICSD #166384; $CaCO_3$), lime (ICSD #75785; CaO), and larnite (ICSD #79550; Ca_2SiO_4) are significant crystalline phases (Fig. 3). These chemical compositions of GBOs are highly similar to granulated coal ash (GCA) (Asaoka et al., 2017), and cement (Marques et al., 2006).

CaO in XRF is usually expressed as a combination of CaO and $CaCO_3$ in XRD analysis (Le et al., 2021). XRD showed that SiO_2 and CaO in GBO11 account for relatively higher ratios than those of GBO31 and GBO13. The low peaks in the GBOs represent minimal quantities that can not be identified by the reference code or overlap with other peaks (Roychand et al., 2020). The crystalline phase tendencies of the GBOs differed depending on the mixing ratio of CBA to OS. Although the Ca_2SiO_4 peak in GBO11 showed many low peaks due to the combination of calcium and silica from CBA and OS, the peaks of $CaCO_3$ and CaO were remarkable. The peaks of $CaCO_3$ and SiO_2 were higher in GBO13 and GBO31, respectively, because of the high CBA and OS mixing ratios.

As reported in a previous study (Table 2) (Jeong and Kim, 2022), XRF analysis indicated that the chemical composition of GBO11 was analogous to that of Portland cement (Ma et al., 2019). As a result, GBO11 is a more suitable mixture to cause a pozzolanic reaction. In contrast, the chemical composition of GBO13 and GBO31 differed when compared to GBO11 and Portland cement in terms of CaO and SiO_2.

3.2. Changes in compressive strength

The compressive strength results for the GBOs from day 14–42 are shown in Fig. 4. During this period, the compressive strength increased from 0.26 MPa to 0.48 MPa in GBO13, from 0.42 MPa to 0.93 MPa in GBO11, and from 0.26 MPa to 0.35 MPa in GBO31. The compressive strength of GBO11 increased significantly by 119% on day 42 compared with initial values on day 14. Although the compressive strength in GBO13 and GBO31 increased slightly after 42 days of curing, their compressive strengths were significantly lower than GBO11 ($p < 0.05$). The compressive strength of an FM reported by Luukkonen et al. (2020) was 1 MPa, indicating that GBO11 exhibits comparable compressive

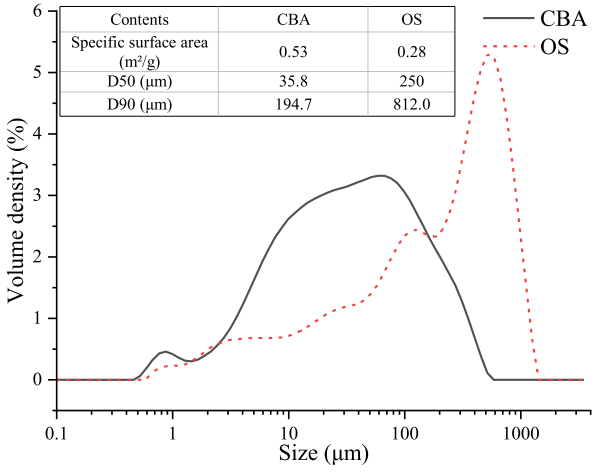

Fig. 2. Particle size distribution and particles' physical properties of pulverized CBA and OS. D50 and D90 represent 50% and 90% of particles in CBA and OS smaller than the measured diameter.

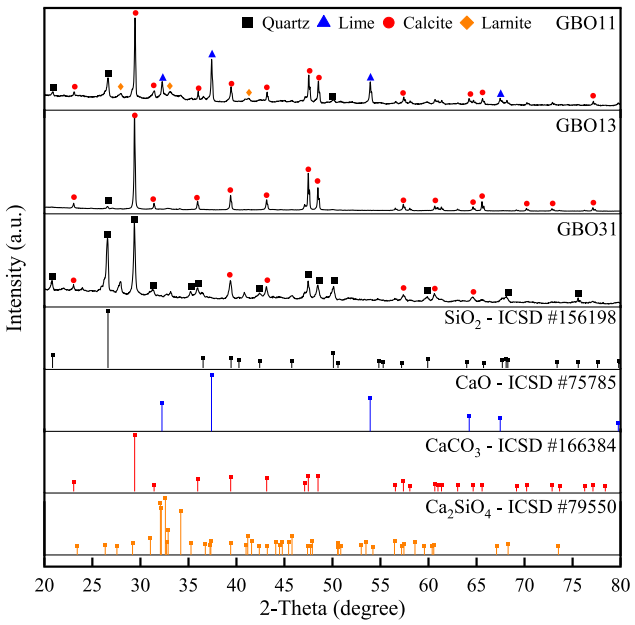

Fig. 3. XRD pattern of GBOs; XRD patterns compared against ICSD reference pattern for individual chemicals.

Table 2
The chemical composition of GBOs and Portland cement.

Content	CaO	SiO_2	Al_2O_3	Fe_2O_3	MgO	TiO_2	SO_3	K_2O
GBO13 (%)	82.8	8.6	3.6	2.0	1.2	0.3	0.8	0.2
GBO11 (%)	61.5	20.9	8.3	4.4	2.2	0.8	1.0	0.5
GBO31 (%)	39.9	33.8	13.0	7.0	2.0	1.2	1.0	0.9
Portland cement (%)	61.4	21.5	5.8	2.9	2.4	0.3	2.4	0.6

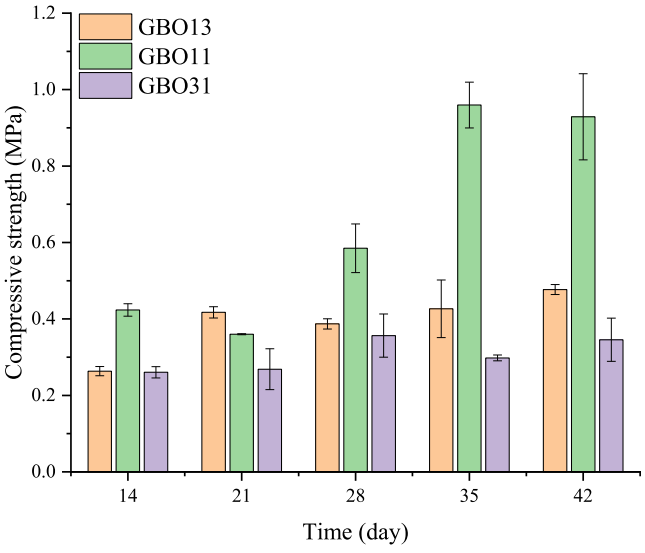

Fig. 4. Changes in compressive strength of GBOs.

strength to their FM.

The high compressive strength of GBO11 was attributed to the formation of cementitious material calcium-silicate-hydrate (C–S–H) through a pozzolanic reaction (Liang and Wang, 2013). An appropriate CBA and OS mixing ratio in GBO11 would have actively facilitated the pozzolanic reaction. In contrast, the compressive strength of GBO13 remained higher than that of GBO31 after 21 days. The strength of OS with a larger particle size distribution than that of CBA should have influenced the relatively high compressive strength of GBO13. The higher specific surface area of CBA (0.53 m^3/g) compared to that of OS (0.28 m^3/g) would have caused high water adsorption (Hasim et al., 2022), contributing to a lower hydration process and decreasing the compressive strength of GBO31. The lowest compressive strength of GBO31 is also supported by the previous studies that reported that the high mixing ratio of CBA for the pozzolanic process resulted in lower compaction and reduction of tensile strength in concrete (Gooi et al., 2020; Hasim et al., 2022).

The compressive strengths of two of the three GBOs were markedly lower than 1 MPa. The D50 of cement is 14.77 μm, whereas the D50 of the GBOs ranges from 280 to 300 μm. The large particle size in the GBOs may have significantly delayed the pozzolanic reaction, contributing to the low compressive strength. However, CBA and OS are porous materials that can easily cause a pozzolanic reaction by transferring water. This can also negatively impact the pozzolanic reactions. The high water-absorption properties of CBA and OS may have caused a slow hydration reaction and inhibited the pozzolanic reaction (Hasim et al., 2022; Kuo et al., 2013). This may impede the filling of the C–S–H gels inside the FM pores (Chen et al., 2019). The fixed amount of water used in the experiment contributed to the low hydration process in the GBOs owing to a shortage of continual water flow (Hasim et al., 2022).

Because of the porosity, a high replacement of CBA and OS in concrete increases the proportion of capillary pores and decreases the volume density (Al Biajawi et al., 2022; Kuo et al., 2013; Naqi et al., 2020; Singh and Siddique, 2015). In addition, the low density of the sample can cause the high lateral tension around the pores in an FM to increase under compression (Ankur and Singh, 2021; Ranjbar and Kuenzel, 2017), generating local fractures around the pores (Ranjbar et al., 2016).

Therefore, a balanced mixing ratio of GBO11 is necessary to reduce the adverse effects of porosity on CBA and OS, and increases the compressive strength by causing a sufficient pozzolanic reaction. This result is supported by previous studies showing that excessive replacement of CBA or OS in concrete decreases compressive strength (Al Biajawi et al., 2022; Kuo et al., 2013).

3.3. Selection of GBO11 for up-flow column filtration experiment

The high compressive strength of GBO11 is similar to that of a filter material developed for water purification in a previous study (Luukkonen et al., 2020). This indicates that GBO is sufficiently strong for use in wastewater treatment. In addition, Jeong and Kim (2022) reported that GBO11 effectively remediated contaminated coastal sediments. However, their study did not consider the changes in the PO_4–P fixation amount in GBO11.

Considering the remediation effects and compressive strength of GBO11, we selected this FM for subsequent up-flow column filtration experiments to evaluate its PO_4–P fixation ability.

3.4. Changes in pH, ORP, and PO_4–P in up-flow column filtration experiment

The pH and ORP in the influent were 6.8–7.0, and 208–240 mV, respectively, during the experimental period (Fig. 5a). This indicated that the quality of the influent remained neutral. Furthermore, the ORP stayed constant during the experimental period. In contrast, the pH and ORP of the initial effluent increased severely increased to 10.2 and decreased to 48 mV, respectively. Over the experimental period, with increasing repetition of influent and effluent, the pH decreased to 9.1, and the ORP steadily increased to 207 mV.

The changes in pH and ORP in the effluent indicated calcium was eluted from GBO11. Calcium elution promotes the hydrolysis of CaO and increases the pH (Jeong and Kim, 2022). The ORP of the initial effluent was significantly lower than the ORP value of the influent. Because the oxygen supply was restricted to a 6 h hydraulic retention time, reducing substances such as calcium and magnesium may have consumed dissolved oxygen by releasing electrons (Haque and Kwon, 2017).

The PO_4–P concentration of the influent was 25.00–27.00 mg/L constantly throughout the experimental period (Fig. 5b). Meanwhile, the PO_4–P concentration in the effluent increased from 0.55 to 12.50 mg/L. The synergistic effects of precipitation and adsorption by GBO11 decreased the PO_4–P concentration significantly in the effluents (Kim et al., 2020; Tsitouridou and Georgiou, 1988; Vohla et al., 2011).

Based on the properties of CBA and OS, the porosity of GBO11 enhanced the physical adsorption of PO_4–P on the surface (Zhou et al., 2019), and the 61.5% CaO in GBO11 promoted calcium elution due to the increased surface area, thereby increasing the precipitation of PO_4–P.

On the other hand, Ca_2SiO_4 in GBO is related to PO_4–P fixation. According to Eq. (1), dissolution of Ca_2SiO_4 would have increased pH and calcium concentration in column (Traynor et al., 2020). This phenomenon was also observed in the previous study that used the granulated coal fly ash and cement to remove of hydrogen sulfide (Asaoka et al., 2017).

$$Ca_2SiO_4 + 3H_2O \rightarrow 2Ca^{2+} + H_3SiO_4^- + 3OH^- \quad (1)$$

Furthermore, the high pH range of the effluent indicates that the main phosphorus species is HPO_4^{2-} (Trejo-Téllez and Gómez-Merino, 2012), which is involved in the precipitation of calcium phosphate (Gustafsson et al., 2012). Thus, PO_4–P is adsorbed and precipitated as

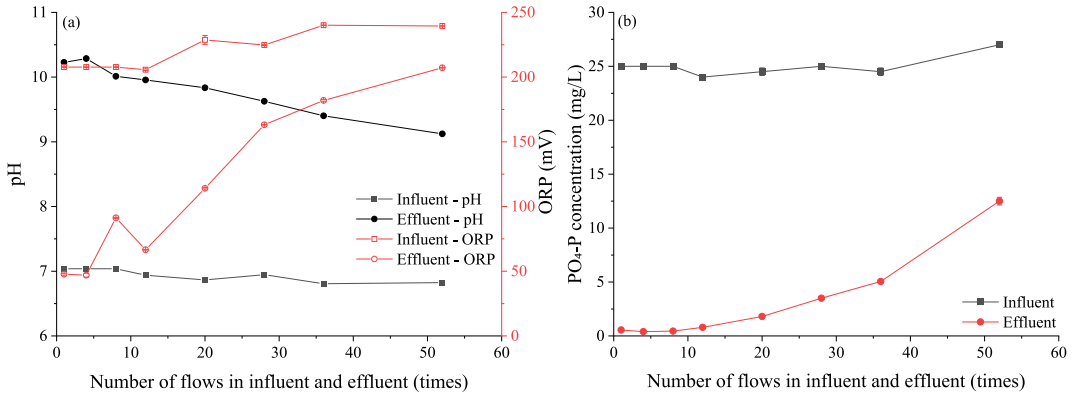

Fig. 5. Changes in the pH and ORP (a), and the PO_4–P concentrations (b) of influent and effluent over repeat cycles through the GBO11-based FM.

hydroxyapatite through the following chemical reaction (Eq. (2)) (Li et al., 2017a).

$$HPO_4^{2-} + 5Ca^{2+} + 4OH^- \rightarrow Ca_5(PO_4)_3OH + 3H_2O \quad (2)$$

3.5. Feasibility of GBO11 as a filtration media

The amount of phosphate fixed by GBO11 decreased from 0.025 to 0.015 mg-P/g throughout the experimental period (Fig. 6). The second polynomial regression equation has a high correlation coefficient of 1.00. Thus, a suitable application period and maximum phosphate fixation amount capacity for GBO11 can be predicted.

The x-intercept of the second polynomial regression equation for the amount of phosphate removed was approximately 86. This provides information on the replacement period for GBO11. In addition, the integral area of the polynomial regression equation between 0 and 86 in the phosphate fixation amount was 1.403 mg/g, which determines the maximum phosphate fixation potential of GBO11.

Most studies on FM have been conducted using a small amount of material in batch experiments, which can easily lead to an overestimation of the amount of phosphate fixation by FM (Vohla et al., 2011). We found several studies on FM having a pellet shape, with phosphate fixation estimates of 0.69–1.98 mg-P/g for coal fly ash pellets (Li et al., 2017b) and 2.05–2.56 mg-P/g for coal ash pellets (Zhou et al., 2019). Although our experiments were performed under different conditions, we demonstrated that GBO11 has a similar phosphate adsorption potential.

In this study, at 25 mg/L, the concentration of PO_4–P in the influent was much higher than the 4–11 mg/L of typical municipal wastewaters (Urdalen, 2013). This would indicate GBO11 has the potential to act as a suitable FM in municipal wastewater and treatment facilities. In addition, the volumetric weight of GBO11 (1140 kg/m^3) is lower than that of gravel (1475 kg/m^3) (Luis et al., 2021), limestone (1190.24 kg/m^3) (Zhou et al., 2019), and fly ash (1324.7 kg/m^3) (Li et al., 2017b), indicating lower potential shipping costs.

4. Conclusion

In this study, we identified a suitable mixing ratio with high compressive strength using CBA and OS, and evaluated the amount of phosphate fixation using the CBA and OS-derived FM. The compressive strength of GBO11 using weight mixing ratio of 1:1 CBA and OS (GBO11) was 0.93 MPa, which was around 2–3 times higher than GBO13 and GBO31. The chemical composition of GBO11 is similar to that of Portland cement. This property promoted the pozzolanic reaction and counterbalanced the adverse effects of porosity on CBA and OS. The maximum PO_4–P fixation potential of GBO11 was 1.403 mg/g, which was attributed to the synergistic effects of precipitation and adsorption. The replacement frequency of GBO11 was approximately 86 cycles.

Based on the compressive strength and phosphate fixation ability of GBO11, its use as an FM looks promising. However, factors affecting its phosphate fixation ability can be influenced by external parameters such as weathering, microorganisms, and influent quality. Therefore, it is necessary to further investigate the realistic phosphate fixation amount and replacement frequency of GBO11 by testing this FM in *in-situ* wastewater treatment facilities.

CRediT author statement

Ilwon Jeong: Conceptualization, Methodology, Validation, Formal analysis, Investigation, Writing - Original Draft, Writing - Review & Editing, Visualization, **Kyunghoi Kim:** Conceptualization, Methodology, Resources, Writing - Original Draft, Writing - Review & Editing, Supervision, Project administration, Funding acquisition.

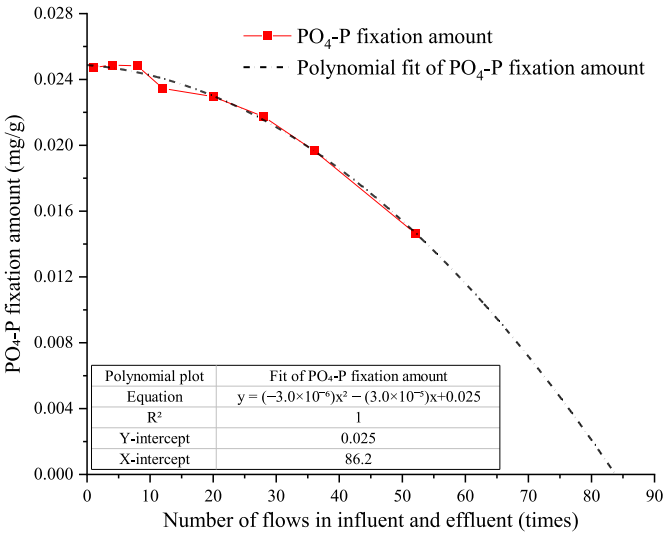

Fig. 6. Changes in the phosphate fixation amount using a second polynomial fit.

Declaration of competing interest

The authors declare that they have no known competing financial interests or personal relationships that could have appeared to influence the work reported in this paper.

Data availability

No data was used for the research described in the article.

Acknowledgments

Funding: This work was supported by the National Research Foundation of Korea [2021R1I1A3060374136178206434010 3].

References

Abbas, S., Arshad, U., Abbass, W., Nehdi, M.L., Ahmed, A., 2020. Recycling untreated coal bottom ash with added value for mitigating alkali–silica reaction in concrete: a sustainable approach. Sustainability 12, 10631.
Abdulmatin, A., Tangchirapat, W., Jaturapitakkul, C., 2018. An investigation of bottom ash as a pozzolanic material. Construct. Build. Mater. 186, 155–162.
Al Biajawi, M.I., Embong, R., Muthusamy, K., Ismail, N., Obianyo, I.I., 2022. Recycled coal bottom ash as sustainable materials for cement replacement in cementitious Composites: a review. Construct. Build. Mater. 338, 127624.
Ankur, N., Singh, N., 2021. Performance of cement mortars and concretes containing coal bottom ash: a comprehensive review. Renew. Sustain. Energy Rev. 149, 111361.
Asaoka, S., Okamura, H., Kim, K., Hatanaka, Y., Nakamoto, K., Hino, K., Oikawa, T., Hayakawa, S., Okuda, T., 2017. Optimum reaction ratio of coal fly ash to blast furnace cement for effective removal of hydrogen sulfide. Chemosphere 168, 384–389.
Blair, T.C., McPherson, J., 1999. Grain-size and textural classification of coarse sedimentary particles. J. Sediment. Res. 69, 6–19.
Bruch, I., Fritsche, J., Bänninger, D., Alewell, U., Sendelov, M., Hürlimann, H., Hasselbach, R., Alewell, C., 2011. Improving the treatment efficiency of constructed wetlands with zeolite-containing filter sands. Bioresour. Technol. 102, 937–941.
Chen, D., Zhang, P., Pan, T., Liao, Y., Zhao, H., 2019. Evaluation of the eco-friendly crushed waste oyster shell mortars containing supplementary cementitious materials. J. Clean. Prod. 237, 117811.
Gooi, S., Mousa, A.A., Kong, D., 2020. A critical review and gap analysis on the use of coal bottom ash as a substitute constituent in concrete. J. Clean. Prod. 268, 121752.
Gustafsson, J.P., Mwamila, L.B., Kergoat, K., 2012. The pH dependence of phosphate sorption and desorption in Swedish agricultural soils. Geoderma 189–190, 304–311.
Haque, N., Kwon, S.-H., 2017. Nutrient dynamics study of overlying water affected by peroxide-treated sediment. Journal of Ecology and Environment 41, 32.
Hasim, A.M., Shahid, K.A., Ariffin, N.F., Nasrudin, N.N., Zaimi, M.N.S., 2022. Properties of high volume coal bottom ash in concrete production. Mater. Today: Proc. 48, 1861–1867.
Hellen, T., Mesquita-Guimarães, J., Henriques, B., Silva, F., Fredel, M., 2019. The potential use of oyster shell waste in new value-added by-product. Resources 8, 1–15.

Jeong, I., Kim, K., 2022. Utilizing a granulated coal bottom ash and oyster shells for nutrient removal in eutrophic sediments. Mar. Pollut. Bull. 177, 113549.
Jeong, I., Nakashita, S., Hibino, T., Kim, K., 2022. Effect of sediment deposition on phosphate and hydrogen sulfide removal by granulated coal ash in coastal sediments. Mar. Pollut. Bull. 179, 113679.
Jeong, I., Woo, H.-E., Lee, I.-C., Yoon, S., Kim, K., 2020. Effects of particle size and pyrolysis temperature of oyster shell on change of coastal benthic environment. Journal of the Korean Society of Marine Environment & Safety 26, 873–880.
Jeong, I.W., Woo, H.E., Lee, I.C., Kim, J.S., Kim, K.H., 2019. Evaluation of nutrients removal using pyrolyzed oyster shells. Journal of the Korean Society of Marine Environment and Safety 25, 906–913.
Kim, K., Kim, K., Asaoka, S., Lee, I.-C., Kim, D.-S., Hayakawa, S., 2020. Quantitative measurement on removal mechanisms of phosphate by Class–F fly ash. International Journal of Coal Preparation and Utilization 40, 892–903.
Kuo, W.-T., Wang, H.-Y., Shu, C.-Y., Su, D.-S., 2013. Engineering properties of controlled low-strength materials containing waste oyster shells. Construct. Build. Mater. 46, 128–133.
Le, T.-T., Park, S.-S., Lee, J.-C., Lee, D.-E., 2021. Strength characteristics of spent coffee grounds and oyster shells cemented with GGBS-based alkaline-activated materials. Construct. Build. Mater. 267, 120986.
Lee, S.W., Kim, Y.M., Kim, R.H., Choi, C.S., 2008. Nano-structured biogenic calcite: a thermal and chemical approach to folia in oyster shell. Micron 39, 380–386.
Li, C., Yu, H., Tabassum, S., Li, L., Wu, D., Zhang, Z., Kong, H., Xu, P., 2017a. Effect of calcium silicate hydrates (CSH) on phosphorus immobilization and speciation in shallow lake sediment. Chem. Eng. J. 317, 844–853.
Li, D.-C., Zhang, Q., Wang, W.-Q., Wang, G.-H., 2022. Filter fabrication by constructing metal-organic frameworks membrane on waste maize straw for efficient phosphate removal from wastewater. Chem. Eng. J. 443, 136461.
Li, S., Cooke, R.A., Wang, L., Ma, F., Bhattarai, R., 2017b. Characterization of fly ash ceramic pellet for phosphorus removal. J. Environ. Manag. 189, 67–74.
Liang, C.-F., Wang, H.-Y., 2013. Feasibility of pulverized oyster shell as a cementing material. Adv. Mater. Sci. Eng. 2013, 809247.
Luis, A., Ana Lorena, E.-G., Amaya, L., Iñaki, T., 2021. Unplanted wetland-type filter for co-treatment of landfill leachate and septic tank wastewater: analysing gravel replacement by plastic and passive (filling-emptied) aeration effects at pilot scale. J. Environ. Manag. 294, 112940.
Luukkonen, T., Yliniemi, J., Sreenivasan, H., Ohenoja, K., Finnilä, M., Franchin, G., Colombo, P., 2020. Ag- or Cu-modified geopolymer filters for water treatment manufactured by 3D printing, direct foaming, or granulation. Sci. Rep. 10, 7233.
Ma, S., Li, W., Shen, X., 2019. Study on the physical and chemical properties of Portland cement with THEED. Construct. Build. Mater. 213, 617–626.
Maeng, J.-H., Kim, T.-Y., Cho, H., Kim, E., 2015. Minimizing environmental impact of ash treatment in thermal power plants (II). Project Report 158–379, 2015.
Marques, S.F., Ribeiro, R.A., Silva, L.M., Ferreira, V.M., Labrincha, J.A., 2006. Study of rehabilitation mortars: construction of a knowledge correlation matrix. Cement Concr. Res. 36, 1894–1902.
Mauclaire, L., Schürmann, A., Thullner, M., Zeyer, J., Gammeter, S., 2004. Sand filtration in a water treatment plant: biological parameters responsible for clogging. J. Water Supply Res. Technol. - Aqua 53, 93–108.
Mustapha, S., Oladejo, T.J., Muhammed, N.M., Saka, A.A., Oluwabunmi, A.A., Abdulkabir, M., Joel, O.O., 2021. Fabrication of porous ceramic pot filters for adsorptive removal of pollutants in tannery wastewater. Scientific African 11, e00705.
Naqi, A., Siddique, S., Kim, H.-K., Jang, J.G., 2020. Examining the potential of calcined oyster shell waste as additive in high volume slag cement. Construct. Build. Mater. 230, 116973.
Ranjbar, N., Kuenzel, C., 2017. Cenospheres: a review. Fuel 207, 1–12.
Ranjbar, N., Talebian, S., Mehrali, M., Kuenzel, C., Cornelis Metselaar, H.S., Jumaat, M. Z., 2016. Mechanisms of interfacial bond in steel and polypropylene fiber reinforced geopolymer composites. Compos. Sci. Technol. 122, 73–81.
Rashidi, N.A., Yusup, S., 2016. Overview on the potential of coal-based bottom ash as low-cost adsorbents. ACS Sustain. Chem. Eng. 4, 1870–1884.
Roychand, R., Kumar Pramanik, B., Zhang, G., Setunge, S., 2020. Recycling steel slag from municipal wastewater treatment plants into concrete applications – a step towards circular economy. Resour. Conserv. Recycl. 152, 104533.
Ruby, C., Barthélémy, K., Hanna, K., Mallet, M., Naille, S., 2015. Synthesis process and hydrodynamic behavior of a new filtration material for passive wastewater dephosphatation. Mater. Des. 86, 168–177.
Shih, P.-K., Chang, W.-L., 2015. The effect of water purification by oyster shell contact bed. Ecol. Eng. 77, 382–390.
Singh, M., Siddique, R., 2015. Properties of concrete containing high volumes of coal bottom ash as fine aggregate. J. Clean. Prod. 91, 269–278.
Traynor, B., Mulcahy, C., Uvegi, H., Aytas, T., Chanut, N., Olivetti, E.A., 2020. Dissolution of olivines from steel and copper slags in basic solution. Cement Concr. Res. 133, 106065.
Trejo-Téllez, L.I., Gómez-Merino, F., 2012. Nutrient Solutions for Hydroponic Systems.
Tsitouridou, R., Georgiou, J., 1988. A contribution to the study of phosphate sorption by three Greek fly ashes. Toxicol. Environ. Chem. 17, 129–138.
Urdalen, I., 2013. Phosphorus Recovery from Municipal Wastewater - Literature Review.
Vidal, B., Hedström, A., Herrmann, I., 2018. Phosphorus reduction in filters for on-site wastewater treatment. J. Water Proc. Eng. 22, 210–217.
Vohla, C., Kõiv, M., Bavor, H.J., Chazarenc, F., Mander, Ü., 2011. Filter materials for phosphorus removal from wastewater in treatment wetlands—a review. Ecol. Eng. 37, 70–89.
Wu, F., Yu, Q., Gauvin, F., Brouwers, H.J.H., Liu, C., 2021. Phosphorus removal from aqueous solutions by adsorptive concrete aggregates. J. Clean. Prod. 278, 123933.
Yan, J., Kirk, D.W., Jia, C.Q., Liu, X., 2007. Sorption of aqueous phosphorus onto bituminous and lignitous coal ashes. J. Hazard Mater. 148, 395–401.
Zhou, H., Bhattarai, R., Li, Y., Li, S., Fan, Y., 2019. Utilization of coal fly and bottom ash pellet for phosphorus adsorption: sustainable management and evaluation. Resour. Conserv. Recycl. 149, 372–380.